Anomalous Hall effect in the magnetic Weyl semimetal NdAlGe with plateaus observed at low temperatures

Naoki Kikugawa [1,*], Shinya Uji [2], and Taichi Terashima [2]

[1]*Center for Basic Research on Materials (CBRM), National Institute for Materials Science, 3-13 Sakura, Tsukuba, Ibaraki 305-0003, Japan*

[2]*Research Center for Materials Nanoarchitectonics (MANA), National Institute for Materials Science, 3-13 Sakura, Tsukuba, Ibaraki 305-0003, Japan*

(Received 29 November 2023; accepted 18 December 2023; published 18 January 2024)

In the *R*Al(Si,Ge) (*R*: lanthanides) family, both spatial inversion and time-reversal symmetries are broken. This may offer opportunities to study Weyl-fermion physics in nontrivial spin structures emerging from a noncentrosymmetric crystal structure. In this study, we investigated the anomalous Hall effect (AHE) in NdAlGe via magnetotransport, magnetization, and magnetic torque measurements down to 40 mK (0.4 K for magnetization). The single crystals grown by a laser-heated floating-zone method exhibit a single magnetic phase transition at T_M = 13.5 K, where the T_M is the transition temperature. With the magnetic field parallel to the easy [001] axis, the AHE gradually evolves as the temperature decreases below T_M. The anomalous Hall conductivity (AHC) reaches $\sim$320 Ω^{-1} cm^{-1} at 40 mK in the magnetically saturated state. Except in low-temperature low-field plateau phases, the AHC and magnetization are proportional, and their ratio agrees with the ratios for conventional ferromagnets, suggesting that the intrinsic AHE occurs by the Karplus-Luttinger mechanism. Below $\sim$0.6 K, the curves of Hall resistivity against the field exhibit plateaus at low fields below $\sim$0.5 T, correlating with the plateaus in the magnetization curve. For the first plateau, the magnetization is one order of magnitude smaller than the magnetically saturated state, whereas the AHE is more than half that in the saturated state. This finding under well below T_M suggests that the AHE at the first plateau is not governed by the magnetization and may be interpreted based on a multipole or spin chirality.

DOI: 10.1103/PhysRevB.109.035143

I. INTRODUCTION

Topologically nontrivial phases in condensed matter have attracted much attention recently due to their novel physical properties [1–7]. Weyl semimetals are one such class of materials. These semimetals have band crossings near the Fermi level and host emergent relativistic quasiparticles, namely, Weyl fermions. The Weyl fermions can be realized when either spatial inversion or time-reversal symmetry is broken. Magnetic Weyl semimetals breaking time-reversal symmetry further offer opportunities to study the interplay between magnetic interactions and topologically nontrivial electronic structures; exhibiting novel phenomena such as the anomalous Hall and Nernst effects with no (or negligibly small) magnetization, optical Hall conductivity, and presence of axion insulators, and chiral domain walls [8–12]. These phenomena may provide the basis for the next-generation spintronics applications [13–15].

The *R*Al(Si,Ge) (*R*: lanthanides) family with the space group $I4_1md$ (No. 109) is a new class of magnetic Weyl semimetals where both the inversion and time-reversal symmetries are broken [16,17]. Recent studies have suggested a topological magnetic order in SmAlSi [18] and NdAlSi [19,20], topological Hall effect in SmAlSi [18] and CeAl(Si,Ge) [18,21,22], anomalous Hall and Nernst effects in PrAl(Ge,Si) and NdAl(Si,Ge) [23–25], anomalous thermal conductivity [26], unusual quantum oscillations in NdAlSi [27,28], possible axial gauge fields in PrAlGe [25], domain wall chirality in CeAl(Si,Ge) [22,29], surface Fermi arcs and bulk Weyl fermion dispersion in PrAlGe [30] and NdAlSi [31], and reconstruction of the electronic structure across the magnetic transition in PrAlGe [32].

We focused on NdAlGe in this study. The physical properties of NdAlGe were investigated by several groups using flux-grown crystals [33–36]. Yang *et al.* [34] reported that NdAlGe undergoes two successive magnetic transitions: an incommensurate spin-density-wave transition at T_{ic} = 6.8 K, where the spin structure is predominantly aligned in the (001) direction with small helical canting to the in-plane, and a commensurate ferrimagnetic transition at T_{com} = 5.1 K, where the spin structure becomes a down-up-up structure propagating in [110] or [1$\bar{1}$0] direction. The polarized up-up-up structure in high fields is formed through a metamagneticlike behavior under a magnetization of $\sim$3 T. Dhital *et al.* reported slightly different transition temperatures T_{ic} = 6.3 K and T_{com} = 4.9 K [36]. The anomalous Hall effect (AHE) was observed in both the down-up-up and polarized regions. This finding contrasts with the fact that the AHE was not detected in a sister material, NdAlSi [34]. Yang *et al.* argued that the AHE in the down-up-up and polarized regions was governed by an intrinsic and extrinsic origin, respectively, whereas Dhital *et al.* proposed an intrinsic origin of both regions [34,36]. Two other research groups also grew NdAlGe crystals by a flux method, but they

*kikugawa.naoki@nims.go.jp

observed a single magnetic transition at 5.2 K [33] or 6 K [35]. Thus, we see that flux-grown crystals exhibit considerable sample dependence.

Recently, we have succeeded in growing the single crystals of NdAlGe by a laser-heated floating-zone technique [37]. This technique can minimize accidental contamination by impurities, allowing us to study the intrinsic properties of NdAlGe. We describe magnetotransport and magnetic torque measurements down to 40 mK, and magnetization ones to 0.4 K. We observed that AHE develops below a single magnetic transition temperature. We argue that, in all regions except a low-temperature low-field region, the observed AHE can be ascribed to the intrinsic Berry curvature and is consistent with the Karplus-Luttinger theory developed for ferromagnets [38]. At low temperatures and under low fields, the Hall conductivity versus magnetic field curves exhibit plateaus. A large AHE is observed at the first plateau, despite low magnetization. We discuss the possible explanations for this phenomenon.

II. EXPERIMENTAL DETAILS

Single crystals of NdAlGe were grown by a laser-heated floating-zone method. The detailed growth procedure was described in Ref. [37]. Here, the grown crystals are deficient in aluminum due to the evaporation during growth. This is in sharp contrast to the aluminum-rich crystals that were obtained by flux methods [33–36].

The crystals were cut and polished into rectangles with a typical size of $3.4 \times 0.5 \times 0.4\,\mathrm{mm}^3$ in [100], [010], and [001] directions, respectively. The electrical contacts were spot welded and supported with silver paste. The contact resistances were below 0.1 Ω. The magnetoresistivity and Hall resistivity were measured simultaneously using a low-frequency (∼13 Hz) ac method. The measurements were performed in a top-loading ^{3}He - ^{4}He dilution refrigerator at temperatures (T) down to 40 mK with sweeping magnetic field (H) between −17.5 and +17.5 T. The electrical current and magnetic field were applied in the [100] and [001] directions, respectively, unless specified otherwise. Because the misalignments of the contact electrodes can cause mixing of the magnetoresistivity and Hall resistivity, the magnetoresistivity (ρ_{xx}) and Hall resistivity (ρ_{yx}) were obtained by symmetrizing $\rho_{xx} = [(\rho_{xx}^{\mathrm{exp}}(H) + \rho_{xx}^{\mathrm{exp}}(-H)]/2$ and antisymmetrizing the experimental data $\rho_{yx} = [(\rho_{yx}^{\mathrm{exp}}(H) - \rho_{yx}^{\mathrm{exp}}(-H)]/2$, respectively.

The magnetic torque (τ) was measured using a capacitive cantilever method in a top-loading ^{3}He - ^{4}He dilution refrigerator. Because the magnetic torque vanishes for symmetric directions, the measurements were performed under the magnetic field applied 3° off from the exact [001] to [010] direction.

The isothermal magnetization (M) measurements under $H \parallel [001]$ between −16 and +16 T were performed down to 2 K using the options of Physical Property Measurement System (PPMS, Quantum Design). The measurement at 0.4 K was performed using the Magnetic Property Measurement System (MPMS3, Quantum Design) with a ^{3}He cooling option. The specific heat (C_P) under zero field was measured down to 0.4 K using the options of Physical Property Measurement System (Quantum Design). The measurement was performed by a relaxation method.

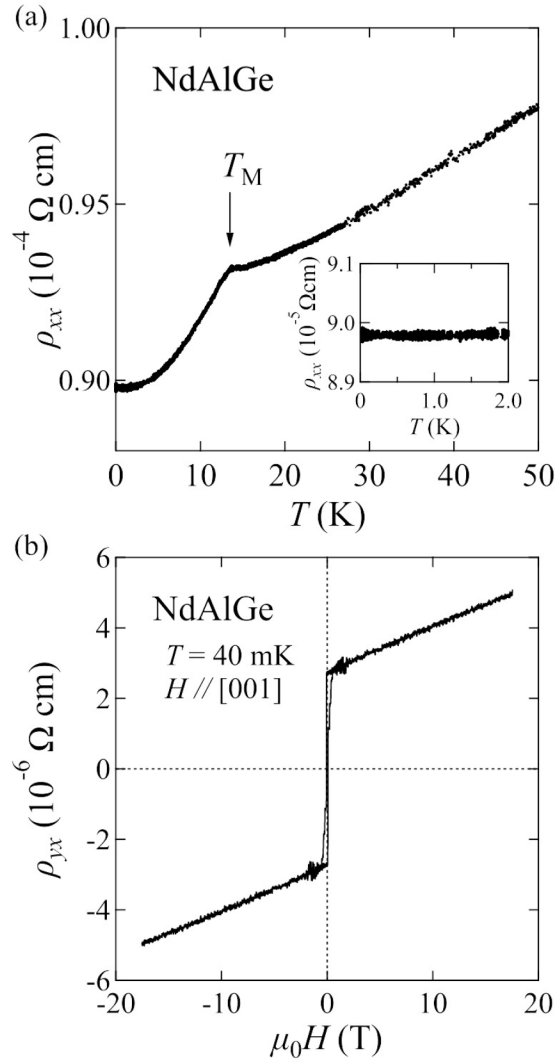

FIG. 1. (a) Temperature dependence of resistivity ρ_{xx} in NdAlGe under zero magnetic field. The current flows in the [100] direction. The inset shows the closeup of the resistivity between 40 mK and 2 K. (b) Hall resistivity ρ_{yx} of NdAlGe at 40 mK under the magnetic field between −17.5 and +17.5 T. The ordinary Hall coefficient $R_0 = +1.28 \times 10^{-3}\mathrm{cm}^3/\mathrm{C}$ is evaluated from the slope of the ρ_{yx} above 1 T.

III. RESULTS

Figure 1(a) shows the temperature (T) dependence of resistivity ρ_{xx} under zero field. A clear kink observed at 13.5 K corresponds to the magnetic ordering temperature (T_M). The inset of Fig. 1(a) shows a closeup of ρ_{xx} below 2 K, where no anomalies are seen down to 40 mK. This finding is consistent with the specific-heat measurement of our floating-zone NdAlGe crystal down to 0.4 K (see Fig. S1 in the Supplemental Material [39]), revealing a single sharp transition at T_M. Notably, the transition width of the specific-heat jump at T_M is as sharp as 0.4 K, suggesting that the floating-zone crystal in this study is highly homogeneous. In comparison, two successive transitions were observed at lower temperatures (∼5 K

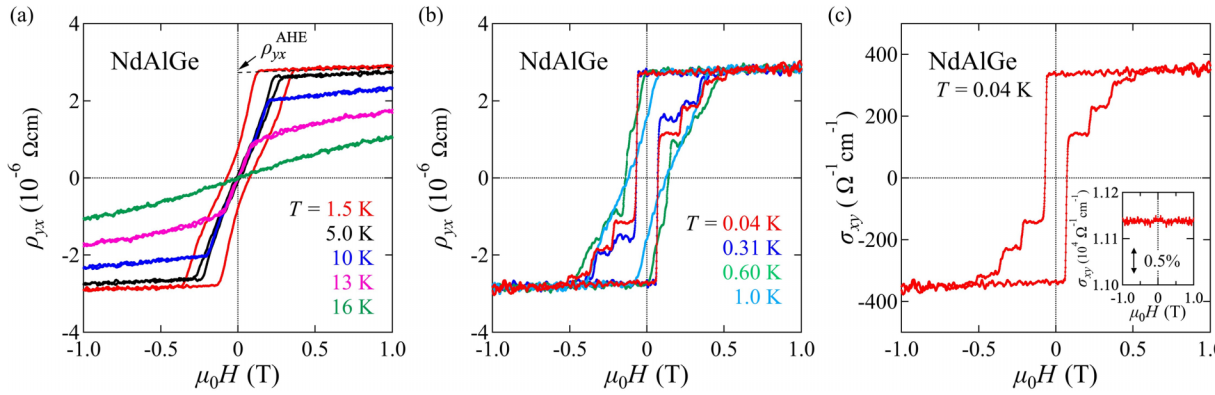

FIG. 2. Hall resistivity ρ_{yx} of NdAlGe at several temperatures (a) between 1.5 and 20 K across the magnetic ordering temperature T_M = 13.5 K, and (b) below 1 K. The magnetic fields are applied along the [001] direction. The anomalous Hall resistivity ρ_{yx}^{AHE} at high temperatures is defined by the extrapolations of the Hall resistivity from a high to zero magnetic field, as shown in (a). (c) Hall conductivity $\sigma_{xy} = \rho_{yx}/(\rho_{xx}^2 + \rho_{yx}^2)$ of NdAlGe at 40 mK. The inset presents the magnetoconductivity $\sigma_{xx} = \rho_{xx}/(\rho_{xx}^2 + \rho_{yx}^2)$.

and ∼6 − 7 K) [34,36], or a single transition was observed at 5 − 6 K in flux-grown NdAlGe crystals [33,35].

Figure 1(b) shows the Hall resistivity ρ_{yx} at 40 mK in a wide magnetic field (H) range of −17.5 to +17.5 T. Hysteresis appears at low fields (< 0.5 T), which will be detailed below. At $|\mu_0 H| > 1$ T (μ_0: magnetic permeability in vacuum), the ρ_{yx} exhibits a linear field dependence with a positive slope, suggesting that holes are the dominant carrier. The ordinary Hall coefficient (R_0) deduced under high field greater than 1 T is $+1.28 \times 10^{-3}$ cm^3/C. A similar value of $+1.25 \times 10^{-3}$ cm^3/C was obtained for another sample (Fig. S2(a) [39]). The coefficients correspond to a carrier density of +4.88 to +4.99 $\times$ 10^{21} cm^{-3}, assuming a single band. In comparison, larger values of R_0 ranging from +4 to $+7 \times 10^{-3}$ cm^3/C, corresponding to smaller hole densities, were reported for flux-grown crystals [34–36]. The difference of the values is likely related to the fact that while floating-zone crystals are aluminum deficient [37], flux-grown ones are aluminum rich [33–36]. No anomaly was found in ρ_{yx} for fields above 1 T [Fig. 1(b)]; this result is consistent with the magnetization (M) curve of our floating-zone crystal (Fig. S3 [39]) and is in sharp contrast with the fact that ρ_{yx} and M in flux-grown crystals exhibit an anomaly around 3 T [33–36].

Figure 2(a) shows the Hall resistivity ρ_{yx} in a low-field region at selected temperatures between 1.5 K and 20 K. The anomalous Hall contribution is observed below T_M = 13.5 K. The hysteresis between up and down field sweep is obvious below 10 K and is closely linked to the magnetization hysteresis (Fig. S3(a) [39]). We notice the ρ_{yx} exhibits nonlinear behavior in the hysteretic region at 1.5 and 5 K.

Figure 2(b) shows the ρ_{yx} curves below 1.5 K. Clear plateaus are developed in the hysteretic region between −0.5 and +0.5 T as the temperature decreases. As the field is swept from the negative to positive values at the lowest temperature of 40 mK, the ρ_{yx} jumps to the first plateau ($\rho_{yx} = 1.1$ μΩ cm), second ($\rho_{yx} = 1.8$ μΩ cm), and third ($\rho_{yx} = 2.5$ μΩ cm) plateaus at 0.07 T, 0.22 T, and 0.36 T, respectively. Finally, ρ_{yx} reaches 2.7 μΩ cm in the field-induced polarized state above 0.5 T. The plateau behavior in ρ_{yx} below 1 K was reproduced in another sample, and the ρ_{yx} finally reached 2.7 μΩ cm above 0.5 T (Fig. S2(b) [39]). Such plateau behavior has not been reported in the flux-grown crystals. Figure 2(c) shows the Hall conductivity σ_{xy} at 40 mK, calculated using the formula $\sigma_{xy} = \rho_{yx}/(\rho_{xx}^2 + \rho_{yx}^2)$, and the inset shows the behavior of magnetoconductivity $\sigma_{xx} = \rho_{xx}/(\rho_{xx}^2 + \rho_{yx}^2)$. The Hall conductivity σ_{xy} reaches a large value of 320 Ω^{-1} cm^{-1} in the high-field polarized state. For the polarized state of flux-grown crystals, σ_{xy} is ∼1, 030 Ω^{-1} cm^{-1} [36] or 0.5–1.5 $\times$ 10^3 Ω^{-1} cm^{-1} [34]. No anomaly was seen in the magnetoconductivity σ_{xx} in the same field region [inset of Fig. 2(c)].

Figure 3 shows the magnetic field angle dependence of ρ_{yx} at a base temperature of 40 mK. Herein, the field angle (θ) was measured from [001] to [010] (inset of Fig. 3). The curves measured at different angles collapse into a single curve when plotted against $\mu_0 H\cos\theta$. This finding is consistent with the Ising character of the neodymium magnetism in NdAlGe [33–37].

Figure 4 shows the plot of anomalous Hall resistivity (ρ_{yx}^{AHE}) against temperature. Herein, the ρ_{yx}^{AHE} is defined by

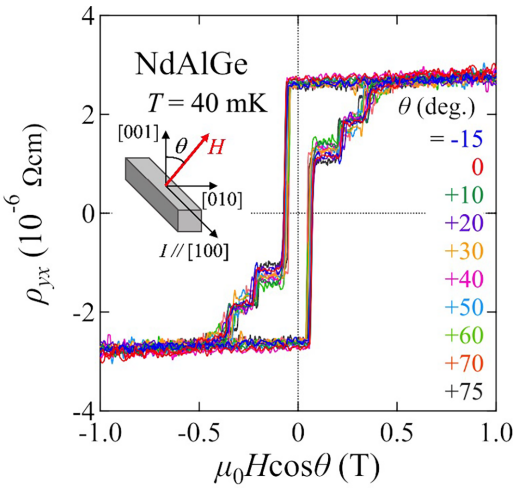

FIG. 3. Magnetic field angle dependence of the Hall resistivity ρ_{yx} in NdAlGe at 40 mK. The field is tilted from the [001] to [010] axes as shown in the inset. The horizontal axis is $\mu_0 H\cos\theta$, where the θ is the tilting angle.

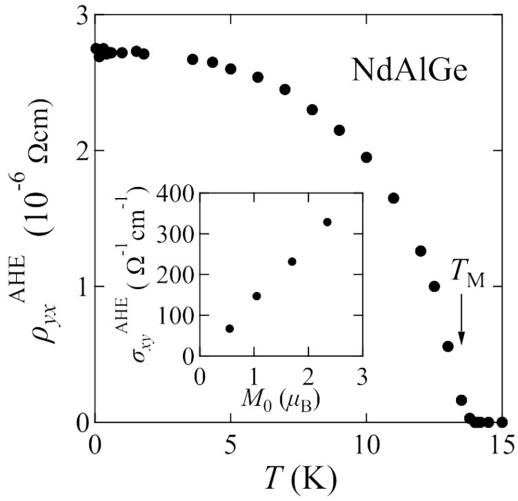

FIG. 4. The anomalous Hall resistivity ρ_{yx}^{AHE} plotted against temperature. The ρ_{yx}^{AHE} gradually evolves below T_{M}. The inset represents anomalous Hall conductivity $\sigma_{xy}^{\mathrm{AHE}}$ against extrapolated zero-field magnetization M_0, obtained by extrapolating the high-field part of a magnetization curve toward zero field (Fig. S3(a) [39]).

the extrapolations of the Hall resistivity from the high to the zero magnetic field for high temperatures, as presented in Fig. 2(a), and it is the residual Hall resistivity at $\mu_0 H = 0$ T for low temperatures [Fig. 2(b)]. The ρ_{yx}^{AHE} gradually evolves below T_{M} and reaches 2.7 $\mu\Omega$ cm at the lowest temperature. The inset of Fig. 4 shows $\sigma_{xy}^{\mathrm{AHE}}$ plotted against extrapolated zero-field magnetization M_0 for four temperatures (T = 2, 10, 12, and 13 K), where M_0 is obtained by extrapolating the high-field part of a magnetization curve toward zero field as presented in Fig. S3(a) [39]. A clear linear relation exists between $\sigma_{xy}^{\mathrm{AHE}}$ and M_0.

Figures 5(a)–5(c) show a comparison of the magnetization M, magnetic torque (τ) divided by magnetic field $\tau/(\mu_0 H)$, and the Hall resistivity ρ_{yx} measured at ∼0.4 K, the lowest possible temperature for magnetization measurements. The magnetic torque is given by $\vec{\tau} = \vec{M} \times \vec{H}$. Considering the Ising nature of the neodymium moments [33–37], $\tau/(\mu_0 H)$ can be roughly approximated to M. Similar to the behavior of ρ_{yx}, as the field is increased from negative to positive values, both M and $\tau/(\mu_0 H)$ exhibit the first and second plateaus before the field-polarized state is reached above 0.5 T. Although the M and $\tau/(\mu_0 H)$ values at the first plateau are close to zero, the ρ_{yx} is more than half of the polarized state (∼1.5 $\mu\Omega$ cm). The transition fields between the three regions slightly differ among the three measurements. This difference is mostly attributed to the sample difference and/or demagnetization factor differences. In addition, only the magnetization curve shows a rather wide transitional (nonflat) region from ∼0.18 to ∼0.28 T between the first and second plateaus. This wide transition region was possibly caused by a temperature instability or increased temperature during the magnetization measurement; the samples were immersed in liquid ^{3}He - ^{4}He mixture for the magnetic torque and ρ_{yx} measurements using the top-loading dilution refrigerator, whereas a sample was held in low-pressure ^{3}He gas atmosphere for the magnetization measurement, and thermal contact was provided

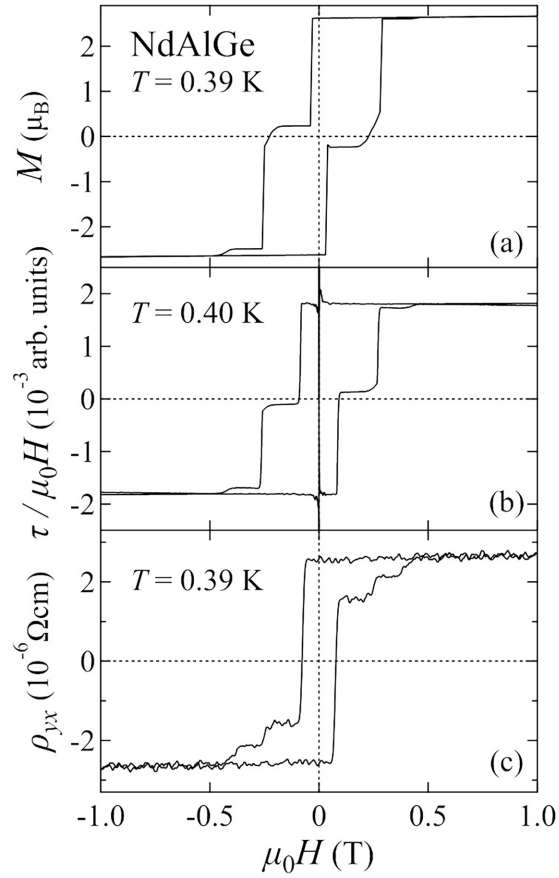

FIG. 5. (a) Isothermal dc magnetization M, (b) magnetic torque (τ) divided by field $\tau/\mu_0 H$, and (c) Hall resistivity ρ_{yx} of NdAlGe at $T \sim 0.4$ K. The plateau structures in the Hall resistivity are closely related to the magnetic properties.

by copper wires attached to the sample. Consequently, the temperature stability and accuracy may be worse in the magnetization measurements.

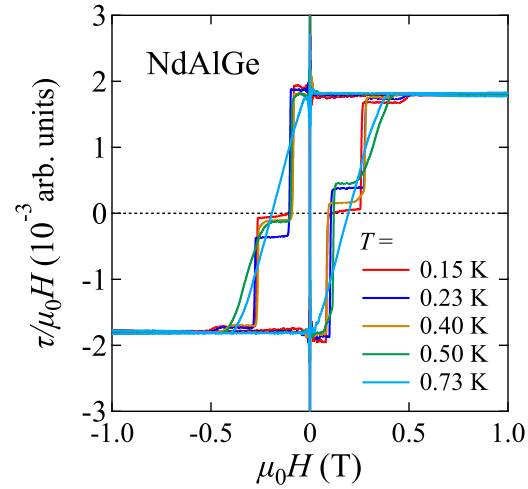

FIG. 6. Magnetic torque divided by the applied field [$\tau/(\mu_0 H)$] below 1 K.

Figure 6 shows the $\tau/(\mu_0 H)$ curves measured at various temperatures below 1.1 K. Similar to the ρ_{yx} data (Figs. 2(b) and S2(b) [39]), the plateaus are sensitive to temperature: the first and second plateaus survive only up to 0.5 and 0.4 K, respectively. The heights of the plateau vary slightly with temperature.

IV. DISCUSSION

We first argue that the observed anomalous Hall conductivity (AHC) $\sigma_{xy}^{\mathrm{AHE}} \sim 320\ \Omega^{-1}\ \mathrm{cm}^{-1}$ in the polarized state [Fig. 2(c)] is primarily attributed to the intrinsic Berry curvature. A theoretical scaling relation between σ_{xy} and σ_{xx} [40–42], experimentally supported, indicated three regimes. AHE in each regime is dominated by different mechanisms: in the high-conductivity regime ($\sigma_{xx} > 10^6\ \Omega^{-1}\ \mathrm{cm}^{-1}$), skew scattering dominates AHE and $\sigma_{xy}^{\mathrm{AHE}} \propto \sigma_{xx}$; in the good-metal regime (σ_{xx} is $10^4 - 10^6\ \Omega^{-1}\ \mathrm{cm}^{-1}$) where the intrinsic Berry-phase contribution dominates and $\sigma_{xy}^{\mathrm{AHE}}$ is approximately independent of σ_{xx}; in the bad-metal regime ($\sigma_{xx} < 10^4\ \Omega^{-1}\ \mathrm{cm}^{-1}$) where $\sigma_{xy}^{\mathrm{AHE}} \propto \sigma_{xx}^{1.6}$. The AHC in the good-metal regime is of the order of $10^2 - 10^3\ \Omega^{-1}\,\mathrm{cm}^{-1}$. Our results ($\sigma_{xx} \sim 1.1 \times 10^4\ \Omega^{-1}\ \mathrm{cm}^{-1}$ and $\sigma_{xy}^{\mathrm{AHE}} \sim 320\ \Omega^{-1}\ \mathrm{cm}^{-1}$ at $T = 40$ mK) perfectly fit the good-metal regime. The intrinsic Berry curvature contribution to the AHE in the polarized state of NdAlGe was theoretically calculated as $\sigma_{xy}^{\mathrm{AHE}} \sim 200\ \Omega^{-1}\ \mathrm{cm}^{-1}$ [34] or $\sim 270\ \Omega^{-1}\mathrm{cm}^{-1}$ [36]. These values are in good agreement with our experimental values.

Furthermore, according to the Karplus-Luttinger theory of the intrinsic AHE, $\rho_{yx}^{\mathrm{AHE}} \sim \rho_{xx}^2 M$ [38]. Considering $\rho_{xx} \gg |\rho_{yx}|$, this relation indicates that $\sigma_{xy}^{\mathrm{AHE}}$ (approximately equal to $\rho_{yx}^{\mathrm{AHE}}/\rho_{xx}^2$) is proportional to M. The present data nicely satisfy this relation (inset of Fig. 4), further supporting the intrinsic mechanism. For various conventional ferromagnets exhibiting AHE, the ratio $\sigma_{xy}^{\mathrm{AHE}}/M$ is in the range of a few tens to $1 \times 10^3\ \Omega^{-1}\ \mathrm{cm}^{-1}/\mathrm{T}$ (where M is measured in tesla) [10]. For the polarized state of NdAlGe, where $M = 0.45$ T, the ratio is $7.1 \times 10^2\ \Omega^{-1}\ \mathrm{cm}^{-1}/\mathrm{T}$, lying in this empirical range.

Our conclusion regarding the intrinsic AHE agrees with the conclusion drawn from studies on flux-grown crystals by Dhital *et al.* [36]. Conversely, Yang *et al.* [34] observed that the temperature dependence of the AHC in the polarized state of flux-grown crystals differs with the sample and does not follow the magnetization; they argued that AHE in the polarized state of NdAlGe has an extrinsic origin.

Next, we focus on the first plateau in the Hall resistivity. Figure 5 indicates that $\tau/(\mu_0 H)$ and M of the first plateau are close to zero and the magnetization is negative, respectively. Nevertheless, the ρ_{yx} has a substantial value of $\rho_{yx} \sim 1.5\ \mu\Omega\,\mathrm{cm}$, ∼55% of its value in the polarized state and has the same positive sign. For the first plateau, where $M = 0.043$ T, the ratio $\sigma_{xy}^{\mathrm{AHE}}/M$ is $4.3 \times 10^3\ \Omega^{-1}\ \mathrm{cm}^{-1}/\mathrm{T}$, exceeding the aforementioned empirical range.

Recent studies on anomalous Hall antiferromagnets indicated that the contribution of the Berry curvature to AHE is not necessarily controlled by magnetization [10,43,44]. Mn_3Sn, for example, is an antiferromagnet without net magnetization (in the absence of spin-orbit coupling), but it exhibits a large AHE. In the case of such anomalous Hall antiferromagnets, breaking of the time-reversal symmetry that is necessary for AHE and is attributed to the magnetic multipoles composed of multiple atoms [43,44]. Another example is $CoTa_3S_6$ and $CoNb_3S_6$ [45,46]. Arguably, a fictitious magnetic field associated with a scalar spin chirality induces a giant Hall response under the small net magnetization [46].

For flux-grown NdAlGe samples, neutron diffraction measurements were performed, and the low-temperature zero-field spin structure was found to be composed of basically antiferromagnetic spin down-up-up chains along [110] directions. Due to the Dzyaloshinskii-Moriya interaction, a part of the spins exhibits a slight canting from the [001] direction, resulting in a noncollinear spin structure [34,36]. The spin structure at the first plateau of the floating-zone crystals may be a variant with the same down-up-up motif. Determining the exact spin structure to identify the multipole or spin chirality responsible for the AHE of the first plateau is highly desirable.

Finally, we discuss the differences between floating-zone and flux-grown crystals. The floating-zone crystals are aluminum deficient, whereas the flux-grown ones are aluminum rich. This difference likely explains the smaller ordinary Hall coefficient R_0 (larger hole density) in the floating-zone crystals, and may also account for the smaller $\sigma_{xy}^{\mathrm{AHE}}$ in the polarized state of these floating-zone crystals since the theoretical calculations indicate that the AHC caused by Berry curvature decreases with a decrease in the Fermi level [34,36]. Further, because the Ruderman-Kittel-Kasuya-Yosida (RKKY) interaction mediated by itinerant carriers is reasonably assumed to be the primary exchange interaction between neodymium moments, the differences between the magnetic phase diagrams of the floating-zone and flux-grown crystals can be attributed to their different carrier densities.

V. SUMMARY

We performed magnetotransport and magnetic torque measurements down to 40 mK and magnetization ones to 0.4 K on floating-zone single crystals of NdAlGe. We observed only one magnetic phase transition at $T_{\mathrm{M}} = 13.5$ K, in contrast to the two transitions observed in some of the flux-grown crystals [34,36]. The AHE occurred below T_{M}, and the AHC reached $\sim 320\ \Omega^{-1}\ \mathrm{cm}^{-1}$ at 40 mK in the polarized state, comparable to the *ab initio* calculations of the intrinsic Berry curvature contribution [34,36]. A comparison with the theoretical scaling relation between $\sigma_{xy}^{\mathrm{AHE}}$ and σ_{xx} supports the Berry curvature origin of the AHE. A linear relation exists between σ_{xy} and M_0, and their ratio $\sigma_{xy}^{\mathrm{AHE}}/M$ is in the typical range for ferromagnets. These results indicate that the AHE, except for the low-temperature low-field region, occurs within the framework of the Karplus-Luttinger theory. At low temperatures and fields below ∼0.6 K and ∼0.5 T, we observe plateaus in the curves of the Hall resistivity against the field. These plateaus in the Hall resistivity are correlated with the ones in the magnetization curves. In the first plateau, although the magnetization is one order of magnitude smaller than that in the saturated state, we observe a large anomalous Hall resistivity, more than half the value observed in the magnetically saturated state. This imbalance between the anomalous Hall effect and magnetization is analogous to anomalous Hall antiferromagnets such as Mn_3Sn or $Co(Nb, Ta)_3S_6$. This finding

indicates that a multipole or spin chirality governs the AHC in the first plateau, and theoretical work on this topic is necessary in the future.

ACKNOWLEDGMENTS

We acknowledge Takanobu Hiroto for comments and support, Masao Arai, and Jun-ichi Inoue for comments and discussion, Ayumi Kawaguchi, Takashi Kato, Momoko Hayashi, Hitoshi Yamaguchi, Takeshi Shimada, Akira Kamimura, John McArthur, and Noritaka Kimura for support. This work is funded by KAKENHI Grants-in-Aids for Scientific Research (Grants No. 18K04715, No. 21H01033, No. 22H01173, and No. 22K19093), and Core-to-Core Program (No. JPJSCCA20170002) from the Japan Society for the Promotion of Science (JSPS) and by a JST-Mirai Program (No. JPMJMI18A3). MANA was established by World Premier International Research Center Initiative (WPI), MEXT, Japan.

[1] Z. Wang and S.-C. Zhang, Chiral anomaly, charge density waves, and axion strings from Weyl semimetals, Phys. Rev. B **87**, 161107(R) (2013).

[2] A. A. Burkov, Topological semimetals, Nat. Mater. **15**, 1145 (2016).

[3] L. Müchler, H. Zhang, S. Chadov, B. Yan, F. Casper, J. Kübler, S.-C. Zhang, and C. Felser, Topological insulators from a chemist's perspective, Angew. Chem., Int. Ed. **51**, 7221 (2012).

[4] M. Z. Hasan and J. E. Moore, Three-dimensional topological insulators, Annu. Rev. Condens. Matter Phys. **2**, 55 (2011).

[5] Y. Ando, Topological insulator materials, J. Phys. Soc. Jpn. **82**, 102001 (2013).

[6] B. Yan and C. Felser, Topological materials: Weyl semimetals, Annu. Rev. Condens. Matter Phys. **8**, 337 (2017).

[7] N. P. Armitage, E. J. Mele, and A. Vishwanath, Weyl and Dirac semimetals in three-dimensional solids, Rev. Mod. Phys. **90**, 015001 (2018).

[8] N. Nagaosa, T. Morimoto, and Y. Tokura, Transport, magnetic and optical properties of Weyl materials, Nat. Rev. Mater. **5**, 621 (2020).

[9] B. A. Bernevig, C. Felser, and H. Beidenkopf, Progress and prospects in magnetic topological materials, Nat. Rev. Mater. **603**, 41 (2022).

[10] S. Nakatsuji and R. Arita, Topological magnets: Functions based on Berry phase and multipoles, Annu. Rev. Condens. Matter Phys. **13**, 119 (2022).

[11] K. Manna, Y. Sun, L. Muechler, J. Kübler, and C. Felser, Heusler, Weyl and Berry, Nat. Rev. Mater. **3**, 244 (2018).

[12] Y. Okamura, S. Minami, Y. Kato, Y. Fujishiro, Y. Kaneko, J. Ikeda, J. Muramoto, R. Kaneko, K. Ueda, V. Kocsis, N. Kanazawa, Y. Taguchi, T. Koretsune, K. Fujiwara, A. Tsukazaki, R. Arita, Y. Tokura, and Y. Takahashi, Giant magneto-optical responses in magnetic Weyl semimetal $Co_3Sn_2S_2$, Nat. Commun. **11**, 4619 (2020).

[13] F. Giustino, J. H. Lee, F. Trier, M. Bibes, S. M. Winter, R. Valentí, Y.-W. Son, L. Taillefer, C. Heil, A. I. Figueroa, B. Plaais, Q. Wu, O. V. Yazyev, E. P. A. Bakkers, J. Nygård, P. Forn-Díaz, S. D. Franceschi, J. W. McIver, L. E. F. F. Torres, T. Low, A. Kumar, R. Galceran, S. O. Valenzuela, M. V. Costache, A. Manchon, E.-A. Kim, G. R. Schleder, A. Fazzio, and S. Roche, The 2021 quantum materials roadmap, J. Phys. Mater. **3**, 042006 (2020).

[14] Q. L. He, T. L. Hughes, N. P. Armitage, Y. Tokura, and K. L. Wang, Topological spintronics and magnetoelectronics, Nat. Mater. **21**, 15 (2022).

[15] L. Šmejkal, Y. Mokrousov, B. Yan, and A. H. MacDonald, Topological antiferromagnetic spintronics, Nat. Phys. **14**, 242 (2018).

[16] P. Puphal, C. Mielke, N. Kumar, Y. Soh, T. Shang, M. Medarde, J. S. White, and E. Pomjakushina, Bulk single-crystal growth of the theoretically predicted magnetic Weyl semimetals *R*AlGe (R = Pr, Ce), Phys. Rev. Mater. **3**, 024204 (2019).

[17] G. Chang, B. Singh, S.-Y. Xu, G. Bian, S.-M. Huang, C.-H. Hsu, I. Belopolski, N. Alidoust, D. S. Sanchez, H. Zheng, H. Lu, X. Zhang, Y. Bian, T.-R. Chang, H. T. Jeng, A. Bansil, H. Hsu, S. Jia, T. Neupert, H. Lin, and M. Z. Hasan, Magnetic and noncentrosymmetric Weyl fermion semimetals in the *R*AlGe family of compounds (R = rare earth), Phys. Rev. B **97**, 041104(R) (2018).

[18] X. Yao, J. Gaudet, R. Verma, D. E. Graf, H.-Y. Yang, F. Bahrami, R. Zhang, A. A. Aczel, S. Subedi, D. H. Torchinsky, J. Sun, A. Bansil, S.-M. Huang, B. Singh, P. Blaha, P. Nikolić, and F. Tafti, Large topological Hall effect and spiral magnetic order in the Weyl semimetal SmAlSi, Phys. Rev. X **13**, 011035 (2023).

[19] J. Gaudet, H.-Y. Yang, S. Baidya, B. Lu, G. Xu, Y. Zhao, J. A. Rodriguez-Rivera, C. M. Hoffmann, D. E. Graf, D. H. Torchinsky, P. Nikolić, D. Vanderbilt, F. Tafti, and C. L. Broholm, Weyl-mediated helical magnetism in NdAlSi, Nat. Mater. **20**, 1650 (2021).

[20] J.-F. Wang, Q.-X. Dong, Z.-P. Guo, M. Lv, Y.-F. Huang, J.-S. Xiang, Z.-A. Ren, Z.-J. Wang, P.-J. Sun, G. Li, and G.-F. Chen, NdAlSi: A magnetic Weyl semimetal candidate with rich magnetic phases and atypical transport properties, Phys. Rev. B **105**, 144435 (2022).

[21] M. M. Piva, J. C. Souza, G. A. Lombardi, K. R. Pakuszewski, C. Adriano, P. G. Pagliuso, and M. Nicklas, Topological Hall effect in CeAlGe, Phys. Rev. Mater. **7**, 074204 (2023).

[22] M. M. Piva, J. C. Souza, V. Brousseau-Couture, S. Sorn, K. R. Pakuszewski, J. K. John, C. Adriano, M. Côté, P. G. Pagliuso, A. Paramekanti, and M. Nicklas, Topological features in the ferromagnetic Weyl semimetal CeAlSi: Role of domain walls, Phys. Rev. Res. **5**, 013068 (2023).

[23] B. Meng, H. Wu, Y. Qiu, C. Wang, Y. Liu, Z. Xia, S. Yuan, H. Chang, and Z. Tian, Large anomalous Hall effect in ferromagnetic Weyl semimetal candidate PrAlGe, APL Mater. **7**, 051110 (2019).

[24] H.-Y. Yang, B. Singh, B. Lu, C.-Y. Huang, F. Bahrami, W.-C. Chiu, D. Graf, S.-M. Huang, B. Wang, H. Lin, D. Torchinsky, A. Bansil, and F. Tafti, Transition from intrinsic to extrinsic anomalous Hall effect in the ferromagnetic Weyl semimetal $PrAlGe_{1-x}Si_x$, APL Mater. **8**, 011111 (2020).

[25] D. Destraz, L. Das, S. S. Tsirkin, Y. Xu, T. Neupert, J. Chang, A. Schilling, A. G. Grushin, J. Kohlbrecher, L. Keller, P. Puphal, E. Pomjakushina, and J. S. White, Magnetism and anomalous transport in the Weyl semimetal PrAlGe: Possi-

ble route to axial gauge fields, npj Quantum Mater. **5**, 5 (2020).

[26] P. K. Tanwar, M. Ahmad, M. S. Alam, X. Yao, F. Tafti, and M. Matusiak, Gravitational anomaly in the ferrimagnetic topological Weyl semimetal NdAlSi, Phys. Rev. B **108**, L161106 (2023).

[27] J.-F. Wang, Q.-X. Dong, Y.-F. Huang, Z.-S. Wang, Z.-P. Guo, Z.-J. Wang, Z.-A. Ren, G. Li, P.-J. Sun, X. Dai, and G.-F. Chen, New type of quantum oscillations stemmed from the strong Weyl fermions - 4*f* electrons exchange interaction, arXiv:2201.06412.

[28] N. Zhang, X. Ding, F. Zhan, H. Li, H. Li, K. Tang, Y. Qian, S. Pan, X. Xiao, J. Zhang, R. Wang, Z. Xiang, and X. Chen, Temperature-dependent and magnetism-controlled Fermi surface changes in magnetic Weyl semimetals, Phys. Rev. Res. **5**, L022013 (2023).

[29] X. He, Y. Li, H. Zeng, Z. Zhu, S. Tan, Y. Zhang, C. Cao, and Y. Luo, Pressure-tuning domain-wall chirality in noncentrosymmetric magnetic Weyl semimetal CeAlGe, Sci. China, Ser. G: Phys., Mech. Astron. **66**, 237011 (2023).

[30] D. S. Sanchez, G. Chang, I. Belopolski, H. Lu, J.-X. Yin, N. Alidoust, X. Xu, T. A. Cochran, X. Zhang, Y. Bian, S. S. Zhang, Y.-Y. Liu, J. Ma, G. Bian, H. Lin, S.-Y. Xu, S. Jia, and M. Z. Hasan, Observation of Weyl fermions in a magnetic non-centrosymmetric crystal, Nat. Commun. **11**, 3356 (2020).

[31] C. Li, J. Zhang, Y. Wang, H. Liu, Q. Guo, E. Rienks, W. Chen, F. Bertran, H. Yang, D. Phuyal, H. Fedderwitz, B. Thiagarajan, M. Dendzik, M. H. Berntsen, Y. Shi, T. Xiang, and O. Tjernberg, Emergence of Weyl fermions by ferrimagnetism in a noncentrosymmetric magnetic Weyl semimetal, Nat. Commun. **14**, 7185 (2023).

[32] R. Yang, M. Corasaniti, C. C. Le, C. Yue, Z. Hu, J. P. Hu, C. Petrovic, and L. Degiorgi, Charge dynamics of a noncentrosymmetric magnetic Weyl semimetal, npj Quantum Mater. **7**, 101 (2022).

[33] J. Zhao, W. Liu, A. Rahman, F. Meng, L. Ling, C. Xi, W. Tong, Y. Bai, Z. Tian, Y. Zhong, Y. Hu, L. Pi, L. Zhang, and Y. Zhang, Field-induced tricritical phenomenon and magnetic structures in magnetic Weyl semimetal candidate NdAlGe, New J. Phys. **24**, 013010 (2022).

[34] H.-Y. Yang, J. Gaudet, R. Verma, S. Baidya, F. Bahrami, X. Yao, C.-Y. Huang, L. DeBeer-Schmitt, A. A. Aczel, G. Xu, H. Lin, A. Bansil, B. Singh, and F. Tafti, Stripe helical magnetism and two regimes of anomalous Hall effect in NdAlGe, Phys. Rev. Mater. **7**, 034202 (2023).

[35] K. Cho, W. H. Shon, K. Kyoo, J. Bae, J. Lee, C.-S. Park, S. Yoon, B. Cho, P. Rawat, and J.-S. Rhyee, Anisotropic metamagnetic transition and intrinsic Berry curvature in magnetic Weyl semimetal NdAlGe, available at SSRN: http://dx.doi.org/10.2139/ssrn.4217268.

[36] C. Dhital, R. L. Dally, R. Ruvalcaba, R. Gonzalez-Hernandez, J. Guerrero-Sanchez, H. B. Cao, Q. Zhang, W. Tian, Y. Wu, M. D. Frontzek, S. K. Karna, A. Meads, B. Wilson, R. Chapai, D. Graf, J. Bacsa, R. Jin, and J. F. DiTusa, Multi-*k* magnetic structure and large anomalous Hall effect in candidate magnetic Weyl semimetal NdAlGe, Phys. Rev. B **107**, 224414 (2023).

[37] N. Kikugawa, T. Terashima, T. Kato, M. Hayashi, H. Yamaguchi, and S. Uji, Bulk physical properties of a magnetic Weyl semimetal candidate NdAlGe grown by a laser floating-zone method, Inorganics **11**, 20 (2023).

[38] R. Karplus and J. M. Luttinger, Hall effect in ferromagnetics, Phys. Rev. **95**, 1154 (1954).

[39] See Supplemental Material at http://link.aps.org/supplemental/10.1103/PhysRevB.109.035143 for the specific heat down to 0.4 K without magnetic field, the Hall resistivity below 1.1 K to show the sample dependence, particularly the plateau structure, and magnetization under a magnetic field applied along the [001] direction, which includes Refs. [33–36].

[40] S. Onoda, N. Sugimoto, and N. Nagaosa, Quantum transport theory of anomalous electric, thermoelectric, and thermal Hall effects in ferromagnets, Phys. Rev. B **77**, 165103 (2008).

[41] N. Nagaosa, J. Sinova, S. Onoda, A. H. MacDonald, and N. P. Ong, Anomalous Hall effect, Rev. Mod. Phys. **82**, 1539 (2010).

[42] T. Chen, T. Tomita, S. Minami, M. Fu, T. Koretsune, M. Kitatani, I. Muhammad, D. Nishio-Hamane, R. Ishii, F. Ishii, R. Arita, and S. Nakatsuji, Anomalous transport due to Weyl fermions in the chiral antiferromagnets Mn_3X, $X =$ Sn, Ge, Nat. Commun. **12**, 572 (2021).

[43] M.-T. Suzuki, T. Koretsune, M. Ochi, and R. Arita, Cluster multipole theory for anomalous Hall effect in antiferromagnets, Phys. Rev. B **95**, 094406 (2017).

[44] L. Šmejkal, A. H. MacDonald, J. Sinova, S. Nakatsuji, and T. Jungwirth, Anomalous Hall antiferromagnets, Nat. Rev. Mater. **7**, 482 (2022).

[45] N. J. Ghimire, A. S. Botana, J. S. Jiang, J. Zhang, Y.-S. Chen, and J. F. Mitchell, Large anomalous Hall effect in the chiral-lattice antiferromagnet $CoNb_3S_6$, Nat. Commun. **9**, 3280 (2018).

[46] H. Takagi, R. Takagi, S. Minami, T. Nomoto, K. Ohishi, M.-T. Suzuki, Y. Yanagi, M. Hirayama, N. D. Khanh, K. Karube, H. Saito, D. Hashizume, R. Kiyanagi, Y. Tokura, R. Arita, T. Nakajima, and S. Seki, Spontaneous topological Hall effect induced by non-coplanar antiferromagnetic order in intercalated van der Waals materials, Nat. Phys. **19**, 961 (2023).